The impact of finite-depth cylindrical and conical holes in lithium niobate photonic crystals

G. W. Burr,[1] S. Diziain,[2] and M.-P. Bernal[2]*

[1] *IBM Almaden Research Center, 650 Harry Road, San Jose, California 95120 USA*
[2] *Institute FEMTO-ST, Département d'Optique P. M. Duffieux CNRS UMR 6174, Université de Franche-Comté, 16 route de Gray, 25030 Besançon cedex, France*
*maria-pilar.bernal@univ-fcomte.fr

Abstract: The performance of lithium niobate (LN) photonic crystals (PhCs) is theoretically analyzed with transmission spectra and band diagrams as calculated by the 3-D Finite-Difference Time Domain (FDTD) method. For a square lattice of holes fabricated in the top surface of an Annealed Proton-Exchange (APE) waveguide, we investigate the influence of both finite hole depth and non-cylindrical hole shape, using a full treatment of the birefringent gradient index profile. As expected, cylindrical holes which are sufficiently deep to overlap the APE waveguide mode (centered at 2.5μm below the surface) produce transmission spectra closely resembling those predicted by simple 2–D modeling. As the hole depth decreases without any change in the cylindrical shape, the contrast between the photonic pass- and stop-bands and the sharpness of the band-edge are slowly lost. We show that this loss of contrast is due to the portion of the buried APE waveguide mode that passes under the holes. However, conical holes of any depth fail to produce well-defined stop-bands in either the transmission spectra or band diagrams. Deep conical holes act as a broad-band attenuator due to refraction of the mode out of the APE region down into the bulk. Experimental results confirming this observation are shown. The impact of holes which are cylindrical at the top and conical at their bottom is also investigated. Given the difficulty of fabricating high aspect-ratio cylindrical holes in lithium niobate, we propose a partial solution to improve the overlap between shallow holes and the buried mode, in which the PhC holes are fabricated at the bottom of a wide, shallow trench previously introduced into the APE waveguide surface.

OCIS codes: (250.5300) Photonic integrated circuits; (250.3140) Integrated optoelectronic circuits; (130.3730) Lithium niobate;

References and links

1. J. D. Joannopoulos, R. D. Meade, and J. N. Winn, *Photonic Crystals: molding the flow of light* (Princeton University Press, Princeton, NJ, 1995).
2. H. Kosaka, T. Kawashima, A. Tomita, M. Notomi, T. Tamamura, T. Sato, and S. Kawakami, "Superprism phenomena in photonic crystals," Phys. Rev. B **58**, R10096–R10099 (1998).
3. T. Baba and M. Nakamura, "Photonic crystal light deflection devices using the superprism effect," IEEE J. Quantum Electron. **38**, 909–914 (2002).

#91054 - $15.00 USD Received 20 Dec 2007; revised 11 Mar 2008; accepted 11 Mar 2008; published 21 Apr 2008

4. R. W. Ziolkowski and T. Liang, "Design and characterization of a grating–assisted coupler enhanced by a photonic–band–gap structure for effective wavelength–division demultiplexing," Opt. Lett. **22**, 1033–1035 (1997).
5. S. H. Fan, P. R. Villeneuve, J. D. Joannopoulos, and H. A. Haus, "Channel drop filters in photonic crystals," Opt. Express **3**, 4–11 (1998).
6. A. Yariv, Y. Xu, R. K. Lee, and A. Scherer, "Coupled–resonator optical waveguide: a proposal and analysis," Opt. Lett. **24**, 711–713 (1999).
7. M. Notomi, K. Yamada, A. Shinya, J. Takahashi, C. Takahashi, and I. Yokohama, "Extremely large group–velocity dispersion of line–defect waveguides in photonic crystal slabs," Phys. Rev. Lett. **87**, 253902 (2001).
8. L. C. Andreani and M. Agio, "Intrinsic diffraction losses in photonic crystal waveguides with line defects," Appl. Phys. Lett. **82**, 2011–2013 (2003).
9. D. Gerace and L. C. Andreani, "Disorder–induced losses in photonic crystal waveguides with line defects," Opt. Lett. **29**, 1897–1899 (2004).
10. A. Taflove and S. C. Hagness, *Computational electrodynamics: the finite–difference time–domain method*, 3rd ed. (Artech House, Boston, 2005).
11. G. W. Burr, S. C. Hagness, and A. Taflove, "FDTD for Photonics," Chapter 16 of Ref. [10].
12. H. Benisty, D. Labilloy, C. Weisbuch, C. J. M. Smith, T. F. Krauss, D. Cassagne, A. Beraud, and C. Jouanin, "Radiation losses of waveguide–based two–dimensional photonic crystals: Positive role of the substrate," Appl. Phys. Lett. **76**, 532–534 (2000).
13. H. Benisty, P. Lalanne, S. Olivier, M. Rattier, C. Weisbuch, C. J. M. Smith, T. F. Krauss, C. Jouanin, and D. Cassagne, "Finite–depth and intrinsic losses in vertically etched two–dimensional photonic crystals," Opt. Quantum Electron. **34**, 205–215 (2002).
14. R. Ferrini, B. Lombardet, B. Wild, R. Houdre, and G. H. Duan, "Hole depth– and shape–induced radiation losses in two–dimensional photonic crystals," Appl. Phys. Lett. **82**, 1009–1011 (2003).
15. R. Ferrini, R. Houdre, H. Benisty, M. Qiu, and J. Moosburger, "Radiation losses in planar photonic crystals: two–dimensional representation of hole depth and shape by an imaginary dielectric constant," J. Opt. Soc. Am. B **20**, 469–478 (2003).
16. R. Ferrini, A. Berrier, L. A. Dunbar, R. Houdre, M. Mulot, S. Anand, S. de Rossi, and A. Talneau, "Minimization of out–of–plane losses in planar photonic crystals by optimizing the vertical waveguide," Appl. Phys. Lett. **85**, 3998–4000 (2004).
17. T. Baba, A. Motegi, T. Iwai, N. Fukaya, Y. Watanabe, and A. Sakai, "Light propagation characteristics of straight single–line–defect waveguides in photonic crystal slabs fabricated into a silicon–on–insulator substrate," IEEE J. Quantum Electron. **38**, 743–752 (2002).
18. W. Bogaerts, P. Bienstman, D. Taillaert, R. Baets, and D. De Zutter, "Out–of–plane scattering in photonic crystal slabs," IEEE Photon. Technol. Lett. **13**, 565–567 (2001).
19. S. G. Johnson, M. I. Povinelli, M. Soljacic, A. Karalis, S. Jacobs, and J. D. Joannopoulos, "Roughness losses and volume–current methods in photonic–crystal waveguides," Appl. Phys. B **81**, 283–293 (2005).
20. Y. Tanaka, T. Asano, Y. Akahane, B. S. Song, and S. Noda, "Theoretical investigation of a two–dimensional photonic crystal slab with truncated cone air holes," Appl. Phys. Lett. **82**, 1661–1663 (2003).
21. F. Lacour, N. Courjal, M. P. Bernal, A. Sabac, C. Bainier, and M. Spajer, "Nanostructuring lithium niobate substrates by focused ion beam milling," Opt. Mater. **27**, 1421–1425 (2005).
22. M. Roussey, M.-P. Bernal, N. Courjal, D. Van Labeke, and F. Baida, "Electro–optic effect exaltation on lithium niobate photonic crystals due to slow photons," Appl. Phys. Lett. **89**, 241110 (2006).
23. M. Roussey, F. I. Baida, and M.-P. Bernal, "Experimental and theoretical observation of the slow light effect on a tunable photonic crystal," J. Opt. Soc. Am. B **24**, 1416–1422 (2007).
24. J. L. Jackel, C. E. Rice, and J. J. Veselka, "Proton–Exchange for High–Index Waveguides in $LiNbO_3$," Appl. Phys. Lett. **41**, 607–608 (1982).
25. J. A. Roden and S. D. Gedney, "Convolution PML (CPML): an efficient FDTD implementation of the CFS–PML for arbitrary media," Microwave Opt. Technol. Lett. **27**, 334–339 (2000).
26. A. Farjadpour, D. Roundy, A. Rodriguez, M. Ibanescu, P. Bermel, J. D. Joannopoulos, S. G. Johnson, and G. W. Burr, "Improving accuracy by subpixel smoothing in the finite–difference time domain," Opt. Lett. **31**, 2972–2974 (2006).
27. M. Levy, R. M. Osgood, R. Liu, L. E. Cross, G. S. Cargill, A. Kumar, and H. Bakhru, "Fabrication of single–crystal lithium niobate films by crystal ion slicing," Appl. Phys. Lett. **73**, 2293–2295 (1998).
28. A. M. Radojevic, R. M. Osgood, N. A. Roy, and H. Bakhru, "Prepatterned optical circuits in thin ion–sliced single–crystal films of $LiNbO_3$," IEEE Photon. Technol. Lett. **14**, 322–324 (2002).
29. P. Rabiei and W. H. Steier, "Lithium niobate ridge waveguides and modulators fabricated using smart guide," Appl. Phys. Lett. **86**, 161115 (2005).

#91054 - $15.00 USD Received 20 Dec 2007; revised 11 Mar 2008; accepted 11 Mar 2008; published 21 Apr 2008

1. Introduction

Two-dimensional or "slab" photonic crystals (2-D PhCs) are of great interest for a large number of diverse and unique applications in integrated optics [1]. With such devices, light confined in the vertical direction by a planar waveguide can be controlled in terms of propagation direction (superprism effect) [2,3], wavelength selectivity (mux-demux filters) [4,5], group velocity (optical buffering) [6, 7], or other passive functionality simply by fabricating a periodic array of holes within the planar waveguide.

However, such heterostructures tend to suffer from propagation losses that can dramatically modify their desired properties. Such losses are generally classified into intrinsic and extrinsic losses [8,9]. Intrinsic losses, which would be present even in a perfectly fabricated device, result from coupling from the guided mode(s) of the nanostructured planar waveguide into the radiation modes of the surrounding cladding. Although such losses can occur in the lateral plane or "slab" direction if a small number of holes are used, these losses are typically "out-of-plane" losses. In contrast, extrinsic losses occur when light is scattered by fabrication imperfections such as roughness, deviations from a circular hole cross-section, hole-to-hole variations in position and/or diameter, and changes in hole diameter as a function of vertical position (e.g., non-cylindrical holes).

These losses are not trivial to study theoretically, given the large computational burden of full 3-D time-domain simulations [10, 11], and given the large number of slab modes to be covered by a mode-expansion technique [8]. A phenomenological approach was proposed to model out-of-plane losses with the two-dimensional (2-D) Finite-Difference Time Domain (2-D FDTD) method [12]. In this approach, an effective imaginary dielectric constant ε'' was introduced at the air holes, so that the energy loss due to out-of-plane scattering into the vertical dimension could be mimicked by a small amount of absorption within the plane of the 2-D simulation.

This perturbative method, valid for weakly waveguiding heterostructures, made it clear that intrinsic losses increase with the square of the dielectric contrast between the cladding and the core of the waveguide ($(\Delta\varepsilon)^2$). This would seem to make slab structures of low index-contrast preferable, since this choice can reduce these intrinsic out-of-plane losses. However, in order to avoid significant extrinsic losses, extremely deep holes are then required in order to overlap the broad extent of the weakly-confined waveguide mode [13]. Since hole depths are often limited by etching capabilities, a compromise is necessary between the index contrast of the slab and a hole-depth that can fully overlap the guided mode.

Furthermore, for many types of etching processes (reactive ion etching, chemically-assisted ion-beam etching, focused ion beam (FIB)), deep holes are frequently characterized by non-vertical sidewalls. The effect of such a truncated-cylindroconical hole shape has been investigated in terms of intrinsic losses with the same 2-D phenomenological approach described above [14–16]. The photonic crystals studied there were based on etching through planar waveguides based on low index contrast ($\Delta\varepsilon \sim 2$) vertical heterostructures of III-V materials such as GaAs or InP.

For high index contrast ($\Delta\varepsilon \sim 11$) heterostructures such as silicon-on-insulator or air-bridge devices [17], out-of-plane losses are very important (save for those Bloch modes located well below the light line) [18]. The slightest fabrication defect tends to result in high losses, given the strong scaling of scattering with refractive index contrast [12, 19]. Even for small cone angles, theoretical investigations have shown that truncated cone air holes give rise to extrinsic losses due to a coupling between TE-like waveguide modes and TM-like slab modes [20]. These studies were based on three dimensional FDTD (3-D FDTD) calculations, which should be applicable whatever the nature of the waveguides (either high or low index contrast) so long as the lateral discretization is fine enough to resolve the dimensional changes being modelled.

#91054 - $15.00 USD Received 20 Dec 2007; revised 11 Mar 2008; accepted 11 Mar 2008; published 21 Apr 2008

One solution proposed to avoid such cross-coupling losses was to design the heterostructure so as to avoid any overlap between the TE-like waveguide modes and TM-like slab modes [20].

2. Active photonic crystals in Lithium Niobate

The device we are interested in here is an electro-optic photonic crystal modulator fabricated on lithium niobate (LN). Lithium niobate is one of the best known ferroelectric crystals, and is used in numerous electro-optic, nonlinear optic, and other applications. Its unique properties such as high Curie temperature, excellent optical transparency in the visible and infrared, high electro-optic coefficients and nonlinear optical susceptibilities make it an ideal material for electronic, photonic, sensor and micro-electro-mechanical-system applications.

A major problem in working with lithium niobate, however, is its well known resistance to standard machining techniques such as wet etching or reactive ion etching. For the fabrication of photonic devices onto substrates already containing conventional LN waveguides, FIB milling appears to be the most attractive technique for producing submicron-diameter holes of high aspect ratio [21]. Before the FIB milling process, a thin layer of chromium is deposited on the LN substrate in order to avoid charging effects. The PhC holes are then fabricated using a multi-pass milling technique, which helps reduce the re-deposition of material onto the sidewalls that would otherwise lead to conical holes.

Recently we have shown the potential of this type of device by experimentally demonstrating an ultra-compact (13×13 sq.$\cdot\mu$m^2) electro-optic photonic crystal modulator, with a measured electro-optic effect $300\times$ larger than found in bulk lithium niobate [22, 23]. The structure used for that experiment consisted of a 15×15 square array of air holes milled by FIB into an APE gradient-index lithium niobate waveguide. Since this APE waveguide was prepared by annealing for 9 hours at 333°C following 90 minutes of immersion in benzoic acid at 180°C [24] rather than by in-diffusion of titanium, only the TE-like mode can propagate. Thus coupling between the desired TE-like and any nearly-guided, TM-like modes should not be an issue.

However, the maximum index change produced at the surface of the crystal is quite small ($\Delta n \sim 0.03$), resulting in a weak light confinement and a broadly distributed mode. For a diffusion mask of 7μm width, the guided mode is 8μm wide with its centroid located 2.5μm below the surface. However, the holes comprising the photonic crystal have a measured depth of approximately 1–1.5μm and a cylindroconical shape after fabrication by FIB milling, as shown by scanning electron microscope (SEM) images (Fig. 1). Unfortunately, some of the material removed by the focused ion beam tends to re-deposit on the sample, which fills in the holes during fabrication. This re-deposition occurs even more strongly during cross-sectioning, and thus the holes are probably deeper and less conical in shape than they would appear to be from these cross-sections.

The finite depth and conical shape of the holes, combined with the weak confinement of the guided mode, can be expected to lead to out-of-plane extrinsic losses. These losses were believed to be partly responsible for the previously observed discrepancies between measured and theoretical transmission spectra of LN photonic crystal devices [22, 23]. As shown in Fig. 2, the experimentally measured transmission bands tend to be broader than would be expected from the calculated spectra, with much more gradual band-edges. Previously, the possible role of inaccurate hole diameter was investigated using 2-D FDTD simulations with circular holes of randomly-distributed size [23].

In the present work, we extend these investigations and analyze the effects of both hole-depth and hole-shape on out-of-plane losses. Transmission and dispersion frequency curves are calculated by the 3-D FDTD algorithm. While great advances have been made in modal techniques for both intrinsic [8] and extrinsic [9] losses, the birefringent gradient-index profile in an

#91054 - $15.00 USD Received 20 Dec 2007; revised 11 Mar 2008; accepted 11 Mar 2008; published 21 Apr 2008

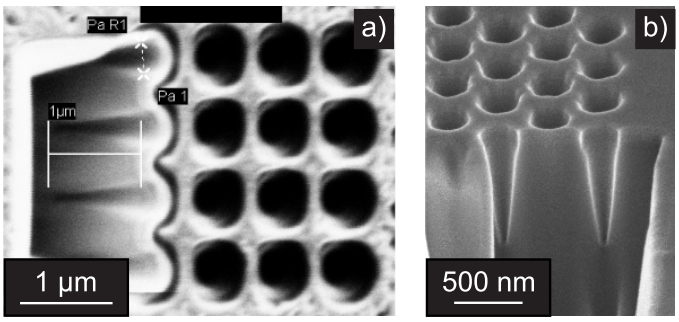

Fig. 1. Scanning electron microscopy images of (a) square lattice and (b) triangular lattice photonic crystals fabricated on lithium niobate. The FIB cross-sections, although distorted by re-deposition during milling, provide qualitative information on the shape and depth of the fabricated holes.

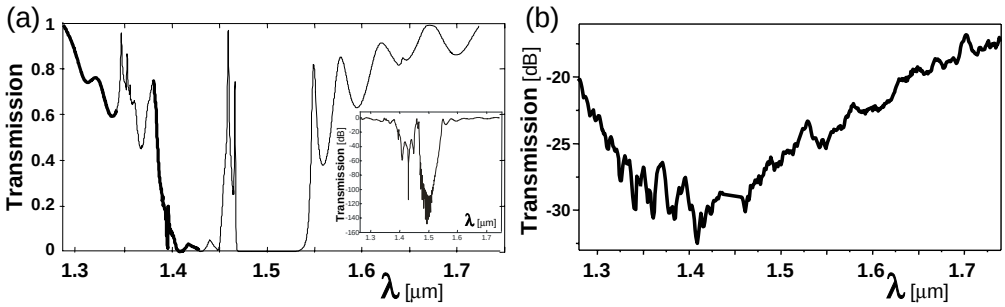

Fig. 2. (a) Theoretical spectra from 2-D FDTD simulations [23] compared with (b) experimentally measured spectra of a square lattice LN PhC [23].

Annealed Proton-Exchange (APE) waveguide represents a more significant challenge for such techniques than a straightforward slab structure. The use of rigorous three dimensional computation tools allows us to treat the system exactly, without the need for assumptions about the modes that will participate in out-coupling, or for any adjustable phenomenological parameters such as ε''.

Our 3-D FDTD method is described in the next section. We validate our approach by comparing the 3–D band diagram we compute for perfectly cylindrical, $>8\mu$m –deep holes with the 2-D band diagram of the same Lithium Niobate PhC (e.g., infinitely deep holes). In the middle sections, we analyze the impact of finite hole-depth and non-cylindrical vertical hole-profile on out-of-plane losses using both transmission spectra and band diagrams. We first explore the impact of finite–depth but cylindrical holes, then the effect of fully conical holes, and finally investigate holes that are cylindrical at the top but conical at the bottom. The finite depth and the cylindrical-conical hybrid shape of the holes are shown to both distort the spectra and reduce the overall transmission, to the point that truly conical holes exhibit no recognizable photonic stop-band at all. We show experimental results to support our conclusion that the conical holes readily refract light out of the weakly guided APE waveguide mode into the substrate. Finally, we propose a partial solution, in which a trench is first introduced into the LN waveguide before fabricating the photonic crystal, in order to allow the subsequently milled holes to reach deeper and more fully overlap the guided mode. We show that while this trench tends to reduce overall transmission, a compromise can be found which retains the sharp spectral features and stop-band of the photonic crystal without too much of a sacrifice in throughput.

#91054 - $15.00 USD Received 20 Dec 2007; revised 11 Mar 2008; accepted 11 Mar 2008; published 21 Apr 2008

3. 3-D FDTD method

The Finite–Difference Time–Domain (FDTD) method has long been used to calculate band diagrams for photonic crystal structures [11]. The approach used here adds only a few modifications in order to incorporate the gradient-index lithium niobate APE waveguide. To simulate a square lattice photonic crystal, the 3-D simulation domain is simply the usual $a \times a$ 2-D unit cell extruded into the third dimension, as shown in cross-section in Fig. 3(a). To correspond to previously measured experimental devices [22, 23], the lattice constant a is 766nm and the hole radius is r/a = 0.27 (207nm). Bloch boundary conditions map the fields at opposing lateral boundaries according to the particular wave-vector being simulated, while Convolution PMLs [25] — placed 2μm above and 8μm below the air–LN boundary, respectively — absorb outgoing radiation.

The curved hole-edges are accurately modelled not only by the choice of a fine cartesian grid-size ($a/24$ laterally along y and z, and $a/14$ vertically along x) but also by a partial-cell technique [26]. This technique, which we have implemented within IBM Almaden's internal FDTD code [11], uses a diagonal tensor approach to correctly model the material distribution in the vicinity of each individual FDTD field component. Thus the birefringence, the gradient index profile, and the curved surface of the hole are all more accurately modelled by this method. The gradient index function modelled here corresponds to an X-cut photonic crystal, with $n_x = n_y = 2.21$ and $n_z = 2.138 + 0.0289 \exp\left(-x^2/2\mu_x^2\right)$ with a characteristic width $\mu_x = 2.5\mu$m, corresponding to the APE waveguides fabricated experimentally [22, 23]. Here we adopt a coordinate system inherited from the underlying crystal structure, where propagation occurs along y, input light is polarized horizontally along z corresponding to the c axis of the lithium niobate crystal, and x represents vertical depth into the substrate.

A spatial and temporal impulse is introduced at a non-symmetry point and the resulting field evolution is collected at a half–dozen monitor points, so that the temporal Fourier transform identifies the eigenfrequencies of the structure at that wave-vector. Repetition of this simulation as a function of the wave-vectors corresponding to the boundary of the first Brillouin zone produces a standard photonic crystal band-diagram as shown in Fig. 3(b). Here, rather than applying a threshold to identify the eigenfrequencies, we plot the raw spectrum with a colorscale normalized to the logarithm of the measured spectral response. While the eigenfrequencies are clearly identifiable here, this raw-spectrum approach will prove useful later on when the mode frequencies are not so clear. These simulations span $200 \times 26 \times 26$ grid-cells, require 64 MB memory (because of the extra partial-cell data), and require approximately 2.5 minutes of computation time each on a 32 dual-processor partition of the BlueGene/L at IBM Almaden.

Figure 3(b) shows the band diagram, as calculated by 3-D FDTD, of a LN PhC with perfectly cylindrical holes etched deep into the substrate ($>8\mu$m). Although a square lattice of air holes does not produce a complete photonic band gap, various stop bands can indeed be found. As an example, along the ΓY direction corresponding to propagation along y at the left side of Fig. 3(b), we can find the region (marked with a box indicating the range from λ=2μm to λ=1μm) that includes the experimental stop-band [22] shown in Fig. 2. From comparison with the band-structure as calculated by 2-D FDTD (Fig. 3(c)), we can conclude that these $>8\mu$m deep holes can be effectively viewed as infinitely deep. For the purposes of later comparison, in Fig. 3(d) we also show the band diagram of un-patterned lithium niobate, e.g., an APE waveguide with no holes milled into it. As expected, no stop bands are observed from bulk material, and mode-splitting due to the birefringence is subtle but observable.

Figure 4(b) shows the simulated transmission as a function of wavelength for 5, 10, 15, 30 and 45 rows of holes. In order to measure transmission spectra, we extend the simulation domain along the y (propagation) direction, as shown in Fig. 4(a). Although the vertical depth of

#91054 - $15.00 USD Received 20 Dec 2007; revised 11 Mar 2008; accepted 11 Mar 2008; published 21 Apr 2008

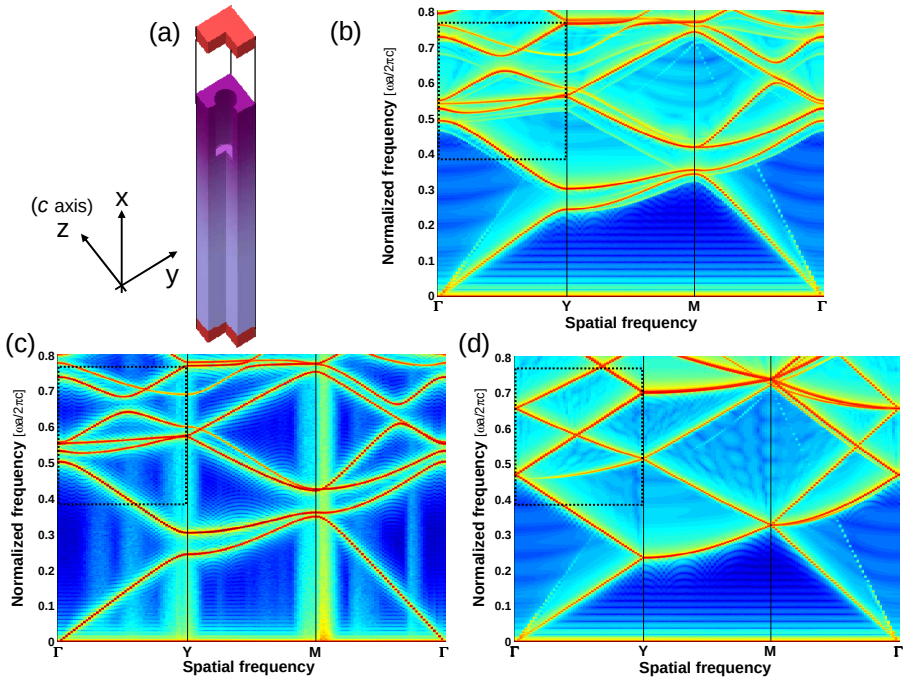

Fig. 3. (a) 3-D unit cell used for FDTD band-diagram computation, composed of a 2-D unit cell extruded vertically through the graded-index top surface of a lithium niobate APE waveguide. The coordinate system is chosen so that the crystal *c* axis intuitively corresponds to *z* and the vertical crystal *a* axis to *x*. (b) 3-D band diagram of a LN PhC with $>8\mu$m deep perfectly cylindrical holes ($a = 766$ nm, $r/a = 0.27$). (c) 2-D band diagram of the same LN PhC. (d) 3-D band diagram of un-patterned lithium niobate with the same APE gradient-index profile. The dotted box shows the span of frequencies corresponding to light between 1 and 2μm (top and bottom, respectively), propagating along the *y* axis (ΓY direction).

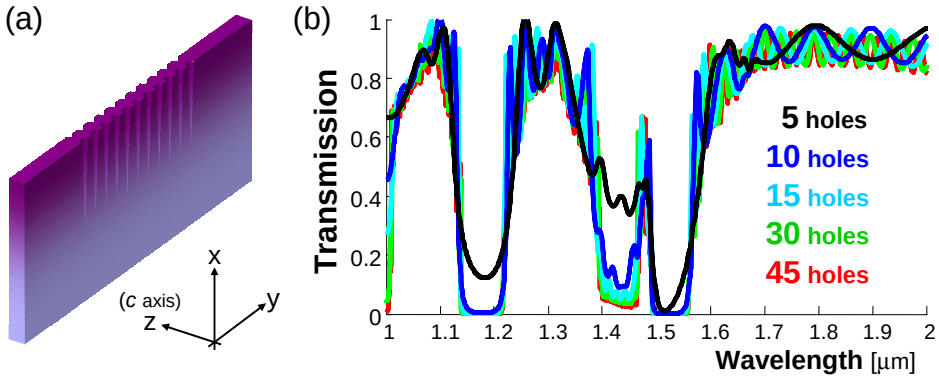

Fig. 4. (a) 3-D unit cell used for FDTD simulations of transmission spectra, which occupies $(na + 12\mu\text{m}) \times 10\mu\text{m} \times a$ for *n* rows of square-lattice photonic crystal at a spacing of *a*=766nm. (b) Transmission spectra of an infinitely-wide lithium niobate photonic crystal composed of 5, 10, 15, 30 and 45 rows of 10μm deep cylindrical holes.

#91054 - $15.00 USD Received 20 Dec 2007; revised 11 Mar 2008; accepted 11 Mar 2008; published 21 Apr 2008

the substrate is extended slightly to 10μm and the *y* boundaries terminated with convolutional PMLs [25], the simulation is still only one lattice period *a* in width along the *x* direction (representing, through periodic boundary conditions, an infinitely wide photonic crystal fabricated on a planar APE waveguide). A Gaussian source (exp $\left(-x^2/2\sigma_x^2 - z^2/2\sigma_z^2\right)$) of height σ_x=1.5μm, nearly uniform along *z* (σ_z=20μm), is introduced just inside one *y* boundary (6μm upstream from the first hole). Transmission spectra are measured just inside the other boundary (12μm downstream after the last hole) over a flux-plane extending from 6μm below up to 0.3μm above the surface. Simulations were typically run with the input Gaussian centered 2.5μm below the substrate surface, although nearly identical results were obtained with source depths ranging between 2 and 3μm .

The grid-spacing is *a*/20 everywhere along *z*, along *y* within 1μm of the holes, and along *x* within 5μm of the substrate, and is *a*/14 elsewhere in the simulation. For our typical simulation containing 30 rows of holes (with buffer, $\sim$33μm total) along the *y* dimension, these simulations span 292 $\times$ 962 $\times$ 22 grid-cells (2 GB memory) and require approximately 30 minutes of computation time each on a 512 dual-processor partition of the BlueGene/L at IBM Almaden.

We now use these 3-D FDTD simulations to examine the expected influence of hole-depth and hole-shape in photonic crystals fabricated within an annealed proton exchange lithium niobate waveguide.

4. Effect of finite hole-depth

Figure 5(a) shows simulated transmission spectra for lithium niobate photonic crystals with 30 rows of cylindrical holes with depths of 1, 2, 2.5, 3, 4, 5, 6, and 8μm, respectively. Holes shallower than 2.5μm do not reach the center of the optical mode, and result in nearly flat transmission spectra without strong spectral features. As the holes become deeper, the contrast and band-edge of the photonic stop-band becomes stronger and sharper. For comparison, we plot in Figs. 5(b) and (c) the ΓY portion of the 3-D band diagrams for 10μm and 2μm deep cylindrical holes as a function of wavelength, over the same wavelength span as Fig. 5(a). (Note that the birefringence of the X-cut lithium niobate causes these bands to differ subtly from those for light propagating along the ΓX direction.) While for 10μm deep cylinders, the stop-band is almost identical to that of the 2-D case, the band diagram for 2μm deep cylinders is a superposition of the bands associated with the square-lattice photonic crystal (Fig. 3(b)) together with the bands associated with the un-patterned APE substrate (Fig. 3(c)). Examination of band-diagrams for intermediate hole depths (not shown) finds both sets of modes present, with the relative strength of the photonic crystal modes increasing (and of the bulk modes decreasing) as the hole depth increases. However, we note that only the relative strength of the photonic crystal modes changes, without significant change in the shape or position of the bands.

By comparing Fig. 4(b) and Fig. 5(a), it becomes clear that the "stop" band near λ=1.45μm builds up relatively slowly with the number of rows, implying a different sort of extinction mechanism. Figure 5(b) shows a mode in the ΓY band diagram within this region of the spectrum, implying that the extinction observed in Fig. 5(a) is associated with efficient coupling from these ΓY modes into other portions of the band diagram, leading to eventual reflection within the first 15 rows of the photonic crystal. We can then surmise that the residual sharp spectral feature just below λ=1.5μm is due light which is transmitted through the photonic crystal by the other limb of this band at low spatial frequencies in Fig. 5(b).

#91054 - $15.00 USD Received 20 Dec 2007; revised 11 Mar 2008; accepted 11 Mar 2008; published 21 Apr 2008

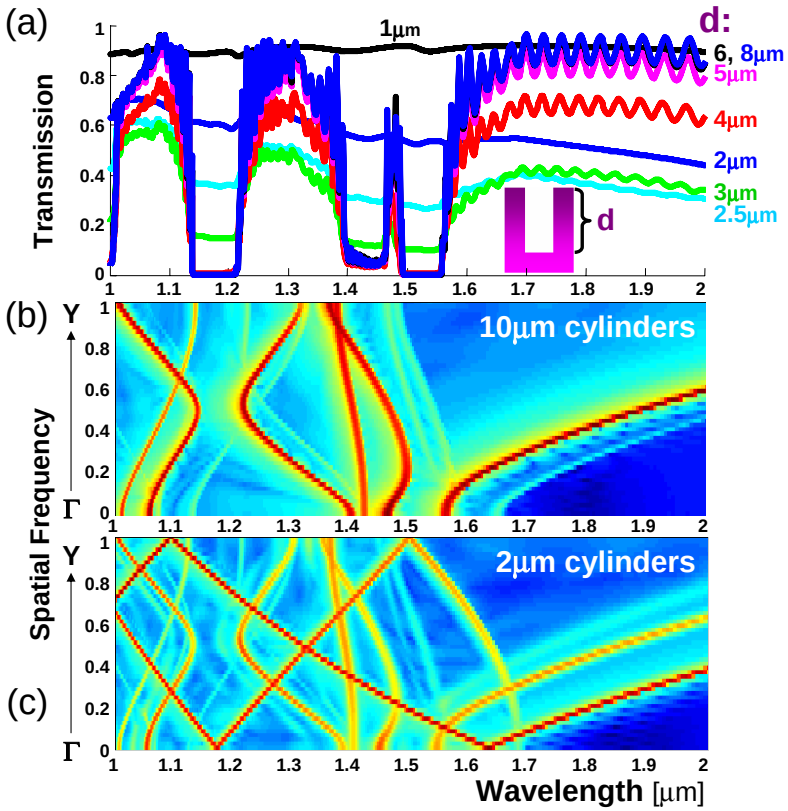

Fig. 5. (a) Transmission spectra of LN PhCs with 30 rows of 1, 2, 2.5, 3, 4, 5, 6 and 8μm deep cylindrical holes. 3-D band diagrams of LN PhCs with (b) 10 and (c) 2μm deep cylindrical holes corresponding to the ΓY direction in the Brillouin zone.

5. Effect of conical hole-shape

Figure 6(a) shows simulated transmission spectra for lithium niobate photonic crystals containing 30 rows of conical holes with depths of 1, 2, 2.5, 3, 4, 5, 6, and 8μm respectively. As opposed to perfectly cylindrical holes, the non-verticality of the sidewalls leads to significant losses. As conical holes are etched deeper, the overall transmission decreases uniformly, with no spectral features that could realistically be considered as a stop-band.

The 3-D band diagrams along the ΓY direction, shown in Figs. 6(b) and (c) for conical holes of 10 and 2μm depth, respectively, confirm these transmission spectra results. For 10μm deep cones, the band structure suggests a superposition of many different band diagrams corresponding to the different r/a ratios, due to the different radii of the cone interacting with the guided optical mode. For 2μm deep cylinders, the band structure is nearly indistinguishable from that of the un-patterned bulk.

Given the large but finite vertical extent of the mode, it can be anticipated that once the conical holes are sufficiently deeply etched, it is not the total depth but the associated sidewall angle (of the top portion that interacts with the mode) which is of importance. Figure 7 plots the transmission spectra for very deep cones, showing that as the sidewall angles become closer and closer to vertical, the expected photonic stop-bands return. However, we note that a sidewall angle of 0.5° or less is required in order to achieve recognizable stop-bands. Interestingly, high contrast extinction is obtained over a broad range of wavelengths for such not-quite-cylindrical

#91054 - $15.00 USD Received 20 Dec 2007; revised 11 Mar 2008; accepted 11 Mar 2008; published 21 Apr 2008

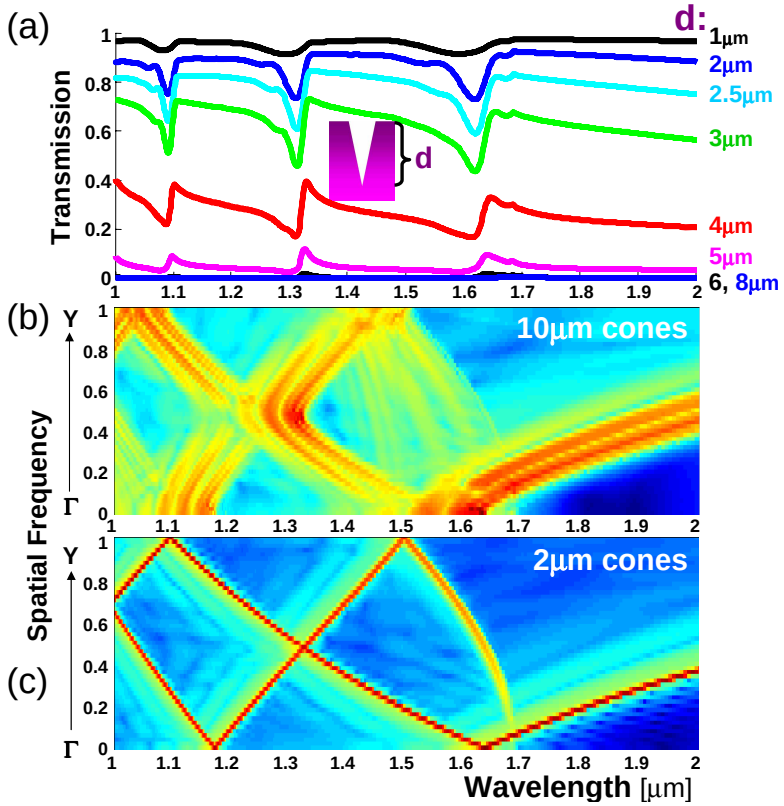

Fig. 6. Transmission spectra of LN PhCs with 30 rows of 1, 2, 2.5, 3, 4, 5, 6 and 8μm deep conical holes. 3-D band diagrams of LN PhCs with (b) 10 and (c) 2μm deep conical holes corresponding to the ΓY direction in the Brillouin zone.

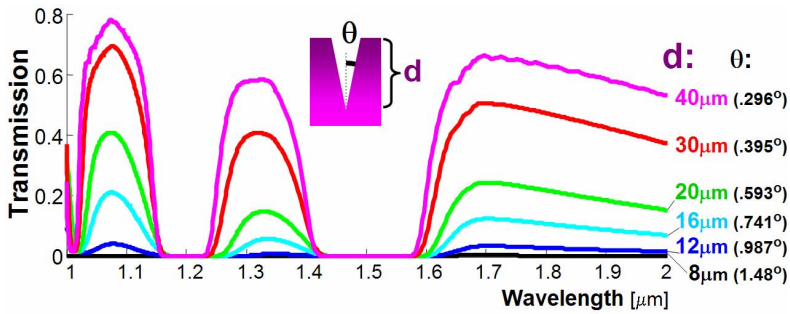

Fig. 7. Transmission spectra of LN PhCs with 30 rows of 8, 10, 12, 16, 20, 30, and 40μm deep conical holes. Also shown are the associated half-cone or sidewall angles θ.

holes.

In order to have a better understanding of light behavior inside the 3-D photonic crystal, we examine the continuous-wave light propagation at a few isolated wavelengths for cylindrical and conical holes of different depths. Illustrative results are shown in Fig. 8. For the case of deep cylinders (Fig. 8(a)-(b)) two wavelengths have been chosen: one inside the stop band (λ=1.520μm, Fig. 8(a)), and one outside (λ=1.570μm, Fig. 8(b)). Because these cylinders are sufficiently deep (10μm) to completely overlap the APE waveguide mode, we observe the

#91054 - $15.00 USD Received 20 Dec 2007; revised 11 Mar 2008; accepted 11 Mar 2008; published 21 Apr 2008

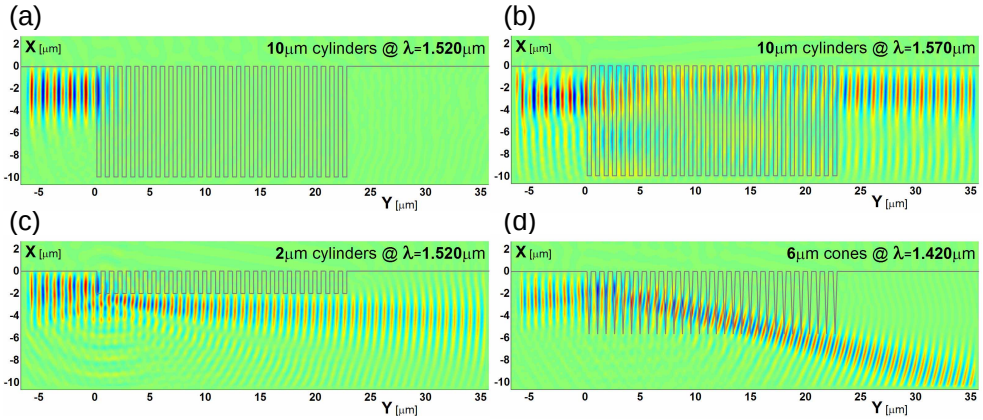

Fig. 8. Continuous field (E_z) slices of LN APE waveguide photonic crystals with (a) deep (10μm) cylinders illuminated at λ=1.520μm, b) deep (10μm) cylinders illuminated at λ=1.570μm, (c) shallow (2μm) cylinders illuminated at λ=1.520μm, and (d) 6μm deep cones illuminated at λ=1.420μm .

expected behavior of light propagation both inside and outside the stop band. Inside the stop-band (λ=1.520μm), light is retro-reflected uniformly from the cylindrical holes, leading to low transmission through the structure. At λ=1.570μm, although Bloch oscillations can be observed within the periodic structure, a significant amount of light is transmitted through the structure and into the un-patterned APE waveguide continuing to the right.

For holes that are insufficiently deep (2μm) and light in the expected stop-band (λ=1.520μm), however, Fig. 8(c) shows that only the portion of the mode which overlaps the holes is retro-reflected. The lower part of the mode passes under the holes without effect and continues as a guided mode of the downstream un-patterned APE waveguide. It can be expected that a significant portion of this transmitted light will redistribute into the original APE modeshape, just as if the original waveguide had been illuminated with a source positioned 4-5μm below the substrate.

However, significantly different behavior is observed in the case of conical holes. Figure 8(d) shows light propagation for 6μm deep cones and a wavelength of λ=1.420μm, although the behavior is qualitatively similar for other wavelengths and cone depths. With cone-shaped holes, incident light is refracted towards the bottom of the substrate. This behavior is not surprising considering the refraction towards the substrate that occurs when light enters each air-filled conical hole from the high-index lithium niobate. And as Fig. 7 shows, just like in slab photonic crystals in III-V semiconductor or Silicon-On-Insulator platforms, these effects eventually go away as the cone angle decreases and the sidewalls become more vertical. What is alarming is the strength of this loss mechanism, and the extreme precision required on slope angles in order to avoid deflecting light out of the APE waveguide. Even the small slope angle (1.5 $^\circ$) associated with an 8μm deep hole is sufficient to allow all of the light to escape the APE waveguide. Thus the usual effects of conical holes are exacerbated by the low-index contrast (and thus weak guiding) of the LN-APE planar waveguide. Together, Figs 6, 7 and 8(d) indicate that for practically achievable etch depths, conical hole shapes must be completely avoided. It is not sufficient to simply etch cone–shaped holes until they overlap the buried guided mode — instead, a sidewall angle within 0.5° of vertical appears to be necessary.

To verify this vertical refraction effect experimentally, we compare the measured transmission through two different LN photonic crystal samples. One sample was fabricated with our

#91054 - $15.00 USD Received 20 Dec 2007; revised 11 Mar 2008; accepted 11 Mar 2008; published 21 Apr 2008

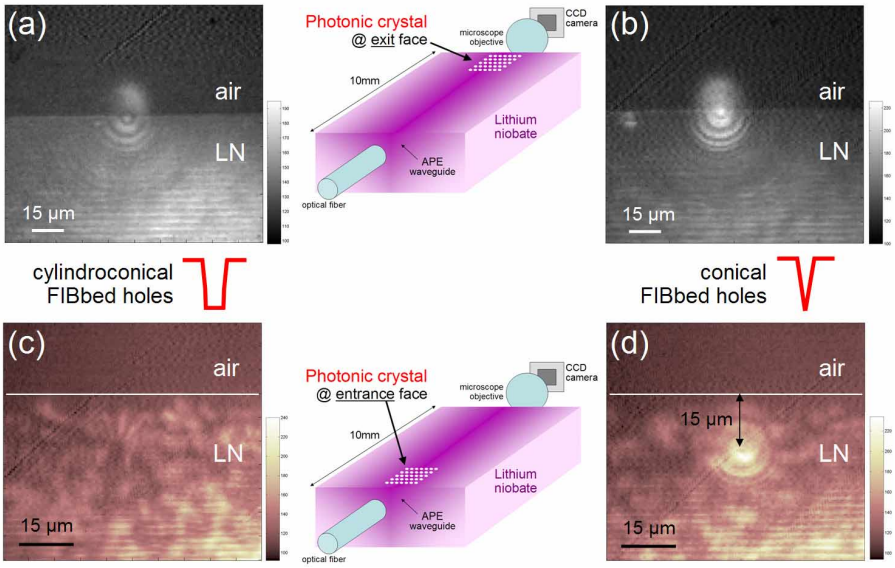

Fig. 9. CCD images of the exit face of LN samples illuminated at a wavelength of 1.55μm, each containing an APE waveguide and a 15 by 15 square lattice photonic crystal fabricated with (a) cylindroconical holes located near the exit face, (b) conical holes located near the exit face, (c) cylindroconical holes located near the entrance face, and (d) conical holes near the entrance face. Not only do the cylindroconical holes (e.g., our best efforts at fabricating cylindrical holes) lead to noticeably better extinction, but conical holes deflect light downward into the substrate — just as predicted by simulation.

standard FIB technique, producing cylindroconical holes as shown in Fig. 1; the other sample was fabricated without the multipass technique, leading to a much more conical shape. Each square lattice photonic crystal of 15 $\times$ 15 holes was fabricated in an APE waveguide approximately 100μm from the edge of the 10mm long sample. With the sample oriented such that the photonic crystal sits at the exit face, Figs. 9(a) and 9(b) compare the results of good and "bad" hole shapes at a wavelength within the empirical stop-band (λ=1.55μm). Here, images of the light at the exit face are produced by a CCD camera and microscope objective. Despite the shallow nature of the fabricated holes, there is noticeably better extinction with the more cylindrical hole.

With the same samples re-oriented so as to illuminate with the photonic crystal near the entrance face, Fig. 9(c) shows the expected good extinction exhibited by the cylindroconical holes. However, Fig. 9(d) demonstrates that, for the sample with intentionally conical holes, the light not only passes through the photonic crystal but is also deflected downwards, exiting nearly 15μm below the top edge of the LN sample. This is the same effect predicted by Fig. 8(d), although because the experimental holes are shallower, the deflection angle is smaller.

Figure 7 suggests two intriguing opportunities, both requiring careful fabrication. One idea would be to intentionally induce a slight non-vertical shape (perhaps in a truncated cone etch) so as to achieve the much broader and deeper stop-bands shown for very deep conical holes. Presumably the low-contrast bands shown in Fig. 5(a) are here improved selectively by increased loss, which is introduced by the additional vertical deflection accumulated during numerous Bloch oscillations back and forth through the periodic structure within this spectral range. For a precisely cylindrical hole, such light would remain guided by the APE waveguide even after repeated oscillations; but for the right cone angle, this light preferentially moves down and

#91054 - $15.00 USD Received 20 Dec 2007; revised 11 Mar 2008; accepted 11 Mar 2008; published 21 Apr 2008

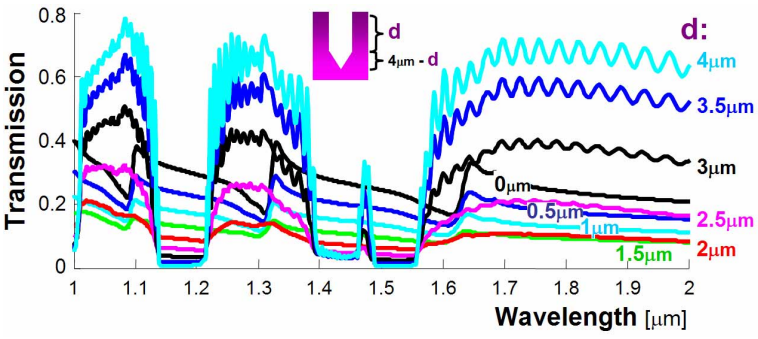

Fig. 10. Transmission spectra of LN PhCs etched by 4μm deep holes that are cylindrical at the top (height d) and conical at the bottom (height (4μm $-d$)).

out of the APE waveguide without significantly affecting the pass-band light which experiences fewer round-trips within the periodic structure. This phenomena effectively attenuates both the weak stop-band near λ=1.45μm , as well as the narrow spectral passband feature near λ=1.5μm previously associated with low spatial frequencies in Fig. 5(b).

The other possibility would be to create a tolerable non-cylindrical shape where the LN-to-air interface (at least in the portion of the hole that interacts with the mode) is angled so as to deflect light up towards the top surface (e.g., a slight barrel shape). One can expect total internal reflection at the top LN-air interface to keep light confined within the substrate over a broad range of refraction angles. While this would likely lead to more extrinsic loss through increased interaction with the surface roughness of the substrate, a more serious drawback is the extreme difficulty of fabricating such structures. One would need to change the tilt of the FIB beam with respect to the substrate during the milling process, to an extent that may be impractical.

Since FIB etching unavoidably produces some amount of conical shape, we investigate the possibility of using holes that are cylindrical for most of their height, with a conical tapering towards the bottom.

6. Effect of a hybrid cylindroconical hole-shape

Here we investigate the expected performance for holes which are etched to a constant depth of 4μm, where the top portion of height d is perfectly cylindrical and the bottom portion is conical over the remaining height $(4\ \mu\text{m} - d)$. In this way, we can vary the cylindrical portion of the holes which will interact with the optical mode. Figure 10 shows the transmission spectra for cylinder lengths from 0 to 4μm varying in steps of 0.5μm . When the cylindrical portion is 3μm or more in depth, the transmission spectra start to exhibit a sharp stop-band with useful contrast and band-edges.

However, it is difficult to fabricate such deep, high-aspect holes in lithium niobate and maintain a near-perfect cylindrical profile over most of the depth. One idea is to remove some portion of the top surface (also using FIB), making a large low-aspect ratio trench or "swimming pool" at the spot where the photonic crystal is to be fabricated. Then one can hope to fabricate slightly shallower sub-micron holes into the bottom of this trench and yet still reach the optical mode.

7. Recessed photonic crystals in LN

It is clear that the presence of a trench in the APE waveguide will itself be a source of radiation losses. Figure 11 shows the calculated transmission spectra, using the same 3-D FDTD for-

#91054 - $15.00 USD Received 20 Dec 2007; revised 11 Mar 2008; accepted 11 Mar 2008; published 21 Apr 2008

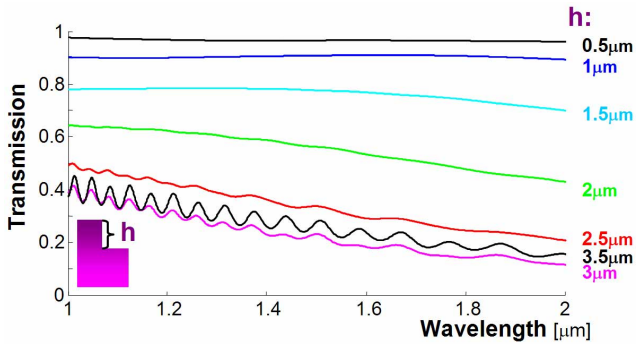

Fig. 11. Transmission spectra of a LN APE planar waveguide with a wide trench of extent 15.3μm (20a) along the propagation direction, for depths varying from 0.5 to 3μm .

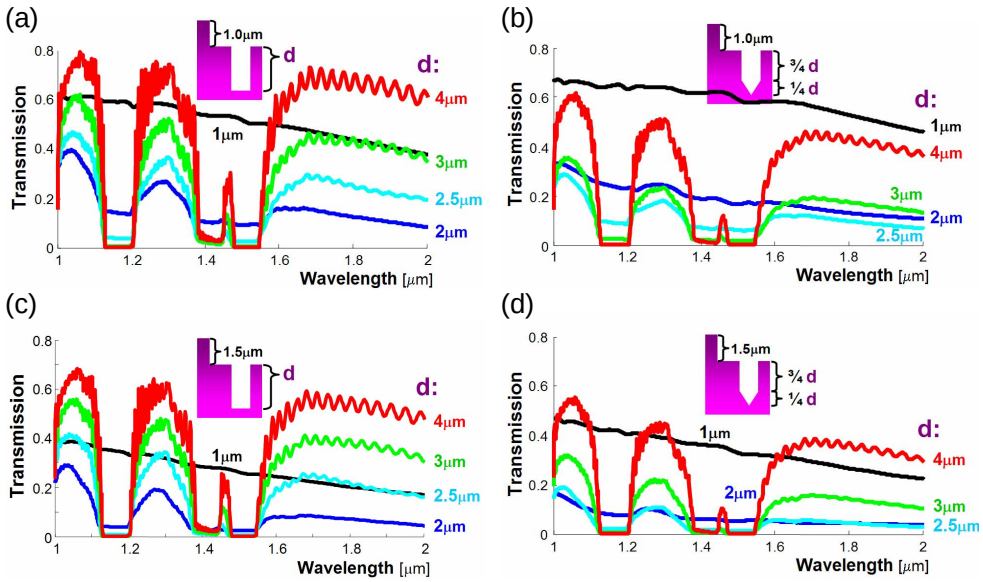

Fig. 12. Transmission spectra of LN PhCs with holes etched into the bottom of a shallow trench. Parts (a) and (b) show the spectra for a 1μm deep trench (extending laterally only 1.5μm (2a) before and after the photonic crystal), for (a) cylindrical holes of depths ranging from 1 to 4μm, and for (a) cylindroconical holes of total depths ranging from 1 to 4μm, where the top 75% of the hole is cylindrical in shape followed by a conical shape over the bottom 25%. Similarly, but for a 1.5μm deep trench, spectra are also shown for (c) cylindrical holes, and for (d) holes which are 75% cylindrical and 25% conical.

malism as before, for light passing through a classical APE waveguide etched with trenches of various depths. We have observed in other simulations (not shown) that losses increase with the length of the trench, implying that the trench should be made only slightly larger than the area of the photonic crystal itself. We also tried using various ramps to produce an adiabatic transition at the upstream edge of the trench (not shown), but all such variants only led to more broadband loss. Thus Fig. 11 shows calculations for trenches with a constant y extent of 15.3μm along the propagation direction (suitable for a photonic crystal of 20 rows) and depths varying from 0.5 to 3μm . We can clearly observe that a deep trench introduces significant insertion loss and reduced contrast for the stop-band. The compromise we choose here is to etch a trench of 1 to

#91054 - $15.00 USD Received 20 Dec 2007; revised 11 Mar 2008; accepted 11 Mar 2008; published 21 Apr 2008

1.5μm in depth, sacrificing approximately 10-25% transmission so that cylinders that extend $\leq$ 3μm into the floor of this trench can then produce acceptable transmission spectra.

Figure 12 shows the transmission spectra as calculated by 3-D FDTD for the combination of a shallow trench and both cylindrical and cylindroconical holes. Figures 12(a) and (b) correspond to a trench of 1μm depth, while Figs. 12(c) and (d) show the results when starting with a 1.5μm trench. In all cases, the trench is 34a in y extent, e.g., with a small buffer of 1.5μm on each side of the 30 rows of photonic crystal. In Figs. 12(a) and (c), the holes are cylindrical and range in depth from 1 to 4μm; in Figs. 12(b) and (d), the holes are cylindrical over the top 75% of their depth, and are conical only over the bottom 25%. Figure 12 compactly illustrates the importance of a cylindrical shape, with even 1μm of conical shape located at a distance of 5μm below the original substrate surface having a significant effect on the contrast between pass- and stop-bands. However, even for a 1μm trench and a cylindroconical hole of 3μm total depth (e.g., cylindrical over the top 2.25μm), a recognizable stop-band can be produced.

8. Conclusion

We have theoretically analyzed the performance of square-lattice photonic crystals fabricated by FIB milling into the top surface of a lithium niobate annealed proton-exchange waveguide. Using a 3-D FDTD algorithm specially adapted to correctly model the birefringent gradient index profile in such devices, we analyzed both transmission spectra and photonic crystal band diagrams. The effects of finite hole depth and non-cylindrical hole shape were investigated. In order to produce transmission spectra that resemble the desired performance represented by a simplistic 2-D model of infinitely deep holes, cylindrical holes should be sufficiently deep to overlap most of the APE waveguide mode in order to achieve high contrast between the photonic pass- and stop-bands and sharp band-edges. Conical holes of any depth fail to produce well-defined stop-bands in either the transmission spectra or band diagrams unless the sidewall angle is within 0.5° of vertical. Interestingly, such slightly tilted sidewalls produce even broader and deeper stop-bands than precisely cylindrical holes. Shallow conical holes act as a broad-band attenuator due to refraction of the mode out of the APE region down into the bulk, an observation which we verified experimentally.

Given the difficulty of fabricating high aspect-ratio cylindrical holes in lithium niobate, we proposed a partial solution to improve the overlap between shallow holes and the buried mode. The fabrication of PhC holes in the bottom of a wide, shallow trench previously introduced into the APE waveguide surface makes it possible for holes of only 3μm depth to produce acceptably sharp and distinct photonic stop-bands.

However, it is clear from this work that the conventional APE waveguide will be extremely susceptible to losses into the substrate due to the weakly guided mode. Other options for conventional waveguides in lithium niobate that could then be combined with photonic crystals would include APE waveguides in thin substrates prepared by crystal ion slicing [27, 28], ridge waveguides etched into lithium niobate [29], and the combination of ridge waveguides of a higher index material such as TiO_2 and APE waveguides.

Acknowledgements

The authors would like to thank Roland Salut (MIMENTO, FEMTO-ST) for fabrication assistance, Diane Reese, Doug DeFrees, Jed Pitera for assistance and support in using the BlueGene/L at the IBM Almaden Research Center, and Nadège Courjal, Matthieu Roussey, and Julien Amet for valuable discussions. GWB would like to thank the CNRS and IBM management for making his extended visit to FEMTO-ST in Besançon possible.

#91054 - $15.00 USD Received 20 Dec 2007; revised 11 Mar 2008; accepted 11 Mar 2008; published 21 Apr 2008